

EFFECT OF RARE EARTH ADDITIONS ON FRACTURE PROPERTIES OF 2.25Cr–1Mo STEELS

HONG Youshi

Institute of Mechanics, Academia Sinica, Beijing, China

W. R. TYSON, B. FAUCHER

Physical Metallurgy Research Laboratories, CANMET, Ottawa, Canada

[Originally published in ACTA METALL SIN (CHINESE EDN) 24 (4) 1988 pp A282–A287.

received 29 October, 1986; in revised form 13 June, 1987]

The inclusion parameters, fracture surface morphology and void growth characteristics of tensile and fracture toughness specimens of 2.25Cr–1Mo steels with and without rare-earth (RE) additions have been investigated by quantitative metallography (QTM), scanning electron microscopy (SEM) and energy dispersive spectroscopy (EDS). There is a substantially higher density of inclusions in the RE-treated steel, which has lower values of fracture properties including critical values of COD and J integral (δ_c and J_{IC}), fracture strain (ϵ_f) and Charpy V-notch energy (CVN). The fracture surface of the RE-treated steel comprises equiaxed dimples of diameters comparable with its inclusion spacing, whereas for the non-RE-treated steels, a wide range of dimple sizes is found with average diameter much smaller than the corresponding inclusion spacing. The investigation indicates that the lower values of fracture properties for the steel with RE at room temperature may be ascribed to its large content of RE-containing inclusions.

KEY WORDS Cr–Mo steel, fracture properties, inclusion parameters, fracture morphology.

The 2.25Cr–1Mo steel has been generally chosen for hydrogenation pressure vessel applications because of its good mechanical properties and resistance to hydrogen and corrosion. However, petrochemical applications require exposure to the temperature range of 400–500°C for thousands of hours and an upward shift in transition temperature as large as 160°C has been reported in 2.25Cr–1Mo steels after prolonged service [1]. Previous research [1,2] has confirmed that rare earth (RE) additions to this steel can suppress its sensitivity to temper embrittlement by forming rare earth compounds that scavenge “tramp” impurities P, Sn, etc. Unfortunately, a reduction in upper-shelf impact energy and an increase in the 50 J transition temperature in RE-treated steels were observed.

In the present study, a further investigation has been carried out on the inclusion distribution parameters, fracture surface

morphology and void growth characteristics of tensile and fracture toughness specimens of 2.25Cr–1Mo steels with and without RE additions. An attempt has been made to relate these microvariables to mechanical properties so as to understand the cause of the lower fracture properties in the steel with RE additions.

1. Experimental procedures and results

1.1 Materials and mechanical properties

Three experimental steels were used. Their chemical compositions are listed in Table 1. The specimens were austenitized at 925°C for 1h and quenched in water, tempered at 675°C for 1.5h and water quenched.

The mechanical properties of these steels at room temperature are given in Table 2. The yield strength σ_y , ultimate strength σ_u and fracture strain ϵ_f were obtained by

Table 1 Chemical composition of steels, wt-%

Code	C	Si	Mn	P	S	Cr	Mo	Ce	La
A	0.12	0.37	0.47	0.005	0.005	2.33	1.01	—	—
B	0.11	0.37	0.46	0.038	0.005	2.25	1.01	—	—
C	0.12	0.48	0.53	0.039	0.002	2.19	0.98	0.115	0.057

Table 2 Mechanical properties of steels

Code	σ_y MPa	σ_u MPa	ε_f	J_{IC} kJ/m ²	δ_c mm	CVN J	SZW μm
A	643	743	1.36	193	0.171	190	67
B	653	744	1.49	169	0.145	175	74
C	607	714	1.14	129	0.111	110	29

conventional uniaxial tensile testing. The fracture properties of J_{IC} , the critical value of J -integral, and δ_c , the critical value of crack tip opening displacement, were measured from three-point-bending tests by a single-specimen unloading technique [3]. The crack orientation is L-T. The Charpy V-notch energy, CVN, was determined according to the ASTM E23 standard. The experimental details were described in [1] and [3].

1.2 Inclusion parameters and distributions

Two-dimensional inclusion parameters and their distributions including density N_2 , diameter D_2 and the nearest neighbour spacing λ_2 were measured on polished samples from 200 fields of $230 \times 180 \mu\text{m}$ each steel, by a Quantimet Image Analyzer. A measuring threshold of $0.145 \mu\text{m}^2$ in area, or $0.43 \mu\text{m}$ in inclusion diameter, was chosen. The corresponding 3-dimensional inclusion size distribution was deduced by the Schwartz-Saltykov method [4]. The 3-D diameter D_3 and 3-D density N_3 were readily obtained from 3-D size distribution results, and the 3-D particle spacing λ_3 was calculated by [4]:

$$\lambda_3 = 0.554 N_3^{-1/3} \quad (1)$$

Fig.1 shows the results obtained for 2-D

and 3-D inclusion parameters, which reveal that the inclusion density N_2 and N_3 of steel C (with RE) is much larger than those for steels A and B (without RE) (Fig. 1a), the average inclusion spacing λ_2 and λ_3 in steel C is smaller than in other steels (Fig.1b), and there is little difference in average inclusion diameter among the 3 steels (Fig.1c).

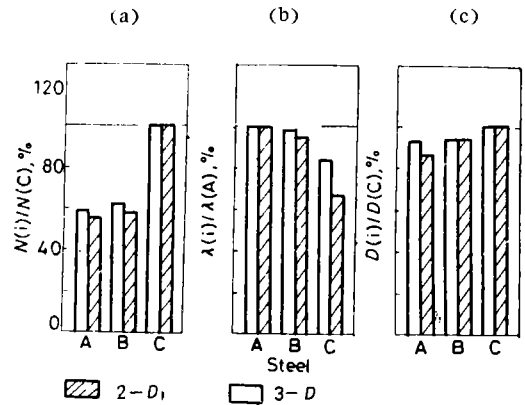


Fig. 1 Comparison of 2-D and 3-D inclusion parameters of steels

(a) Inclusion density, N_2 (C)=732mm⁻², N_3 (C)=3.14×10⁵mm⁻³

(b) inclusion spacing, λ_2 (A)=21.0μm, λ_3 (A)=9.70μm

(c) inclusion diameter, D_2 (C)=1.77μm

D_3 (C)=2.33μm

1.3 Fractography and dimple size distribution

Fracture surfaces of three-point-bend specimens were examined and inclusion chemistry was analyzed by an SEM equipped with an EDS analyzer. It is observed that, between the initiation boundary of a ductile crack and its preceding fatigue pre-crack tip, there is a stretch-zone. The value of stretch-zone width (SZW) was determined by averaging the measurements from 8 SEM photographs (magnification 200×) of each steel. The re-

sults are also listed in Table 2, which indicate that the value of SZW in steel C is much smaller than those in steels A and B.

Fig.2 shows the fracture pattern in ductile crack regions of the steels; all are covered by nearly equiaxed dimples. The dimple sizes of the steels were measured also by QTM from dimple outlines in transparencies traced from SEM photographs taken in ductile crack regions. The dimple size distributions of steels A and C are plotted in Figs.3

and 4. The observations and measurements show that the dimple size in steel C is relatively uniform (Fig.2c) with a smaller range of dimple size distribution (Fig.3), the majority of which are between 6 and 14 μm in diameter (Fig.4). Whereas in steels A and B, there is a wide range of dimple size including a great number of small dimples and a few large ones (Fig.2a and b). Further examinations demonstrate that the distribution parameter

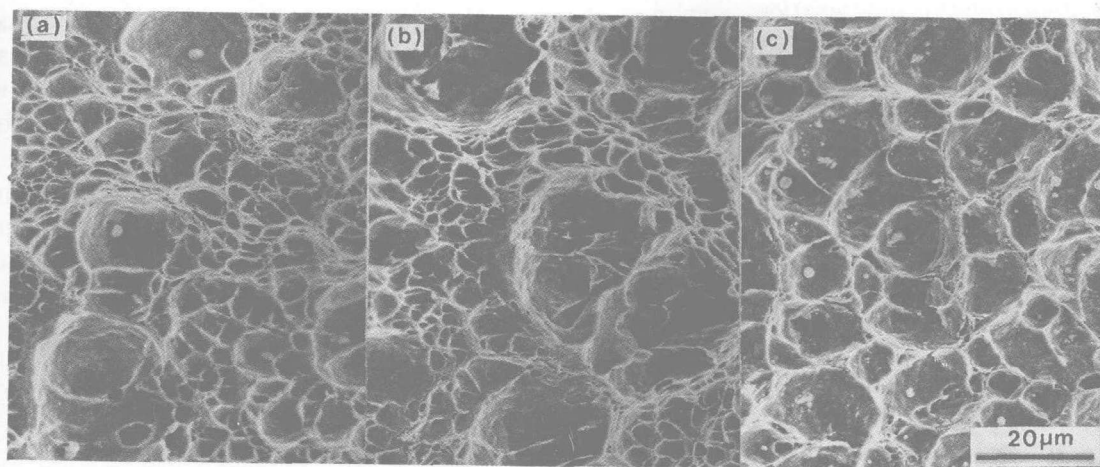


Fig. 2 Fractographs of ductile cracks for steels A (a), B (b) and C (c)

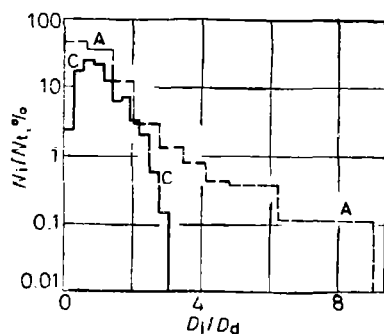


Fig. 3 Dimple size distributions for steels A and C

D_i —dimple diameter; D_d —average dimple dia.,
 N_i —number of dimples at D_i ; N_t —total
 number of dimples; Steel A $D_d = 2.88 \mu\text{m}$;
 Steel C $D_d = 7.17 \mu\text{m}$

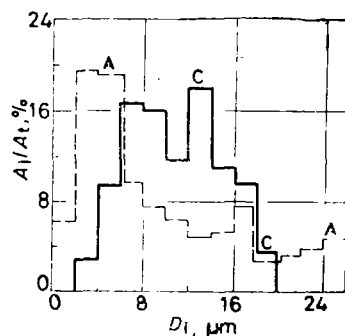


Fig. 4 A_i/A_t vs D_i for steels A and C

A_i —area of dimples at D_i ; A_t —
 total fracture surface area

D_i / D_d is as wide as 9 for steel A (Fig.3) and a large part of fracture surface is covered by small dimples of a diameter less than or equal to $6 \mu\text{m}$ (Fig.4).

The EDS examinations of steels A and B indicated that S, Mn and Al occurred commonly in the inclusions whose compositions were presumably MnS , Al_2O_3 and $\text{MnS} \cdot \text{Al}_2\text{O}_3$. In steel C, Ce and La were detected in most of the inclusions, which were RE-containing inclusions.

1.4 Void growth characteristics

Tensile specimens were sectioned longitudinally and then polished. From these sectioned samples, it is observed that voids initiated from inclusions and grew to a certain extent. Fig. 5 is an SEM photograph of steel C taken on the site of 0.1 mm away from its fracture surface. It is seen that the voids in the middle area coalesced. The size and area fraction of voids decrease with the increasing of the distance away from fracture surface and consequently, the area fraction of voids, f_A , was measured as a function of distance from the fracture surface. The measurements, by QTM, were made on slices, perpendicular to the axial direction, each measurement

consisting of 8 fields of $220 (\text{axial}) \times 180 \mu\text{m}$ (transverse). On the other hand, the current diameter of the specimen at each corresponding point, d_i , was determined with a travelling microscope and the true strain at each point, ε_i , was obtained from:

$$\varepsilon_i = 2 \ln (d_0 / d_i) \quad (2)$$

where d_0 is the initial diameter of the specimen. Fig.6 plots the curves of f_A as a function of ε_i for the steels. It is noted that the measurement for f_A contained the image signals from both voids and inclusions. At the point far away from fracture surface, f_A should approach the 2-D inclusion density; whereas at the point close to fracture surface, f_A is predominantly contributed by voids.

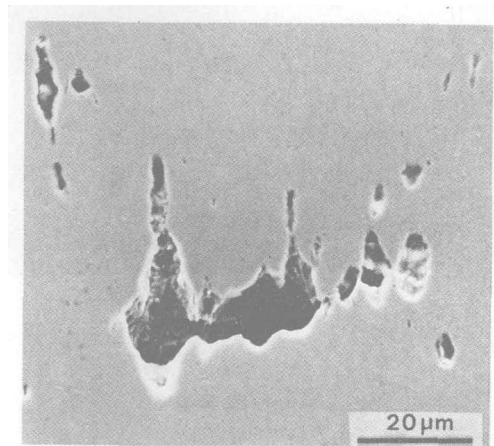


Fig. 5 Voids on sectioned tensile specimen of steel C

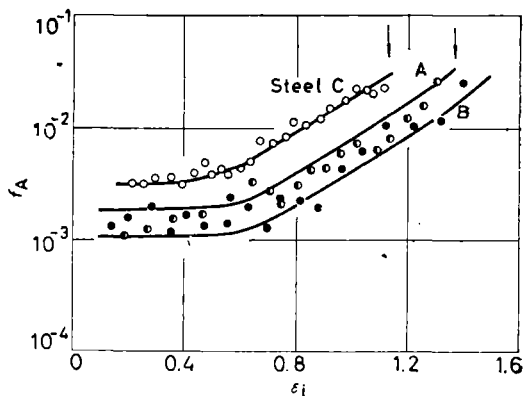


Fig. 6 f_A vs ε_i

2. Discussion

From Tables 1 and 2, it is seen that the fracture properties (ε_f , J_{IC} , δ_c , CVN) of steel C are lower than those of steels A and B. Steel A contains lower P, which is responsible for the difference in fracture properties between steels A and B; whereas the lower fracture properties in steel C, which is RE treated based on the composition of steel B, are obviously a result of the RE additions. Fig.1 shows that the inclusion density of steel C is

40% greater than those of the other steels. Also, the inclusion diameter of the 3 steels are nearly the same, with the result that the inclusion spacing is smaller in steel C. The λ_3 of steel C, 8.16 μm , is close to its average dimple size of 7.17 μm . This approximate agreement and the relatively uniform dimple size, together with the EDS examinations, imply that the numerous RE-containing inclusions are the void-initiation-sources of ductile fracture for steel C.

From Fig.6, it is observed that the variation of f_A with ε_i of steels A and B is within the same scattered band, which indicates that the void initiation and growth characters of the two steels are basically identical. However, the f_A — ε_i curve of steel C is evidently above those of steels A and B. In other words, at the same true strain, steel C contains more void area fraction than those for steels A and B. This suggests that, at the same true strain, there is a greater void-initiation-rate in steel C and its process of void growth and coalescence is always prior to that occurred in steels A and B, which is obviously correlated with the larger inclusion content in it. It is also seen from Fig.6 that, for the 3 steels, although the values of f_A at a given strain are different, their values of f_A at fracture are nearly the same, about 3%. Therefore, steel C, whose f_A is always higher, appears a lower fracture strain than those for the other steels (arrows in Fig.6).

As mentioned in previous section, the fracture surface of steels A and B covered by a large number of small dimples and a few big ones (Figs.2a and b). The result of QTM measurement (Fig.3) reveals that the range of dimple size distribution of steel A extends to $D_1/D_d = 9$. The big dimples in these steels were formed from non-metallic inclusions which are most likely MnS , Al_2O_3 , $\text{MnS} \cdot \text{Al}_2\text{O}_3$, etc. The small dimples, especially those smaller than 4 μm in diameter, may be formed from small particles such as carbides or even from dislocation interactions, which are below the measuring threshold and are excluded in the QTM results. In support of

the notion, the average dimple sizes of steels A and B are much smaller than their average inclusion spacings. In steel A, for instance, the average dimple size is 2.88 μm , whereas its 3-D inclusion spacing is 9.70 μm . In steel C, on the contrary, D_d and λ_3 are comparable, for the dimples were predominantly initiated from RE-containing inclusions, which are included in the QTM measurements.

It is generally assumed that the contour of a root for a blunting crack is a semicircular and consequently, the ratio of δ_c to SZW is about 2. The values of the ratio for steels A, B, and C are 2.6, 2.0, and 3.8, respectively. The first two values are close to the assumed one, but the ratio for steel C is somewhat high. It is also noted that, in all cases, δ_c is about an order of magnitude larger than λ_3 . The ratio of δ_c to λ_3 is found to be between 13 and 18. These figures contrast with the value of 0.7 to 2.5 predicted by the model of Rice and Johnson [5]. Recently, an alternative model for ductile fracture proposed by Bates [6] uses the criterion for crack growth that requires attainment of a critical strain over a distance typically containing several inclusions, rather than the criterion used by Rice and Johnson of linking of a single void with the blunting crack tip. The relation between inclusion parameters and δ_c in light of the alternative theory will be the subject of a further investigation.

3. Conclusions

(1) The major characteristics of the fractography for the RE-treated steel are: smaller SZW and relatively equiaxed dimples of a diameter comparable with its 3-D inclusion spacing. The major characteristics of the fractography for the non-RE-treated steels are: larger SZW and the wide range of dimple size distribution with a smaller average diameter.

(2) At the same true stain, the void area fraction for the RE-treated steel is greater than those for the non-RE-treated steels. The void area fractions at fracture for the steels

with and without RE are all about 3%.

(3) The marked increase in inclusion density resulted from RE additions leads to the significantly lowering in the fracture properties of the RE-treated steel at room temperature.

Acknowledgments — The authors wish to thank Dr. M. Shehata and Mr. B. Casault for their assistance in QTM measurements and Mr. V. Chartrand for his help in SEM observations.

REFERENCES

- 1 Knight R F, Tyson W R, Sproule G I. *Met Technol*, 1984; 11 : 273—279
- 2 Graham M J, Sproule G I, Ho P. *Metall Trans*, 1983; 14A : 2558—2560
- 3 Faucher B, Tyon W R. *In* : Wessel E T, Loss F J eds. *Elastic—Plastic Fracture Test Methods : User's Experience*, ASTM STP 856, 1985 : 278—293
- 4 Underwood E E. *Quantitative Stereology*, Reading, Mass : Addison—Wesley, 1970 : 80—147
- 5 Rice J R, Johnson M A. *In* : Kanninen M F, Adler W F, Rosenfield A R eds. *Inelastic Behaviour of Solids*, New York: McGraw—Hill, 1970 : 641—672
- 6 Bates R C. *In* : Wells J M, Landes J D eds. *Fracture : Interactions of Microstructure, Mechanisms, Mechanics (Conference Proceedings)*, The Metallurgical Society of AIME, 1984 : 117—155

Correspondent : HONG Youshi, Institute of Mechanics, Academia Sinica, Beijing 100080, China